Supporting Information

Chengzhe Liu[a], Yangyang Yu[a], Yuhan Liu[b], Baijun Liu[c], Zhaoyan Sun[d], Guangshan Zhu[a], Wei Hu[a]*

[a] Dr. C. Liu, Dr. Y. Yu, Prof. Dr. G. Zhu, Prof. Dr. W. Hu
Faculty of Chemistry, Northeast Normal University,
5268 Renmin Street, Changchun 130024, P. R. China
E-mail: huw884@nenu.edu.cn
[b] Dr. Y. Liu
Future Technologies Research Department, National Engineering Research Center for Rail Passenger Vehicles, CRRC Changchun Railway Vehicles Co., Ltd.
2001 Changke Road, Changchun 130062, P. R. China
[c] Prof. Dr. B. Liu
College of Chemistry, Jilin University,
2699 Qianjin Street, Changchun 130012, P. R. China
[d] Prof. Dr. Z. Sun
State Key Laboratory of Polymer Physics and Chemistry, Changchun Institute of Applied Chemistry, Chinese Academy of Sciences,
5625 Renmin Street, Changchun 130022, P. R. China

Keywords: PAFs; Hydrogel electrolytes; Dendrite-free; Zinc metal anodes

Experimental Section

Materials

Piperazine, Anhydrous Potassium Carbonate, Cyanuric Chloride, Anhydrous 1,4-Dioxane, are purchased from Beijing Enoke Technology Co., Ltd. Zinc trifluoromethanesulfonate ($Zn(OTf)_2$) was purchased from MacLean Co., Ltd.. Acrylamide (AM) was purchased from aladdin Co., Ltd., and bacterial cellulose (BC) was afforded by Hainan Guangyu Biotechnology Co., Ltd.

Experimental Section

6 mmol of piperazine and 12 mmol of anhydrous potassium carbonate were added to a flask. Then, 50 ml of anhydrous 1,4-dioxane was introduced into the flask under stirring until homogeneous. Under ice-water bath, a mixture of 4 mmol of cyanuric chloride and 20 ml of anhydrous 1,4-dioxane was slowly added to the system via dropping. The reaction mixture was stirred to be homogeneous, and was then reacted at 90 °C for 36 h under oxygen-free conditions. Upon completion of the reaction, the solid product was collected by filtration, and subjected to Soxhlet extraction sequentially with dichloromethane and ethanol. Finally, the product was vacuum-dried at 100 °C for 24 h, denoted as PAF-6.

Preparation of hydrogel electrolytes

To prepare the composite hydrogel electrolyte, 1 g of acrylamide was dissolved in 10 ml of deionized water. 0.2 g of bacterial cellulose and 0.3 g of PAF-6 were immersed in the acrylamide solution. Subsequently, the mixture was maintained at 60 °C for 2 h to initiate the cross-linking to obtain polyacrylamide (PAM)-based hydrogel. Finally, the obtained hydrogel was immersed in 10 mL of 2 M zinc trifluoromethanesulfonate ($Zn(CF_3SO_3)_2$) aqueous solution. PAM/BC hydrogel electrolytes without PAF-6 and PAM hydrogel electrolytes without both PAF-6 and BC were prepared with the same experimental methods.

Mechanical performance

Mechanical properties of hydrogel electrolytes were measured on a universal mechanical tester at a deformation rate of 20 mm min^{-1}. Prior to tensile tests, the hydrogel electrolytes were cut into strips with size of 20×10×2 mm^3. The compressive test was performed by using the cylindrical shaped samples (10 mm in diameter and height).

Chemical structural characterization

The morphology of the samples was inspected on a scanning electron microscope (SEM, JSM-7610FPlus, Japan). Fourier-transform infrared (FTIR) spectra (Brüker VERTEX 70, Germany) were acquired to analyze the chemical components of the samples. The phase structure was revealed by X-ray diffraction (XRD) patterns with a Cu Kα radiation source (Rigaku SmartLab SE, Japan). The specific surface area and pore size distribution were measured on a nitrogen adsorption-desorption instrument (BSD-660, China) at 77 K, and calculated based on the Brunauer-Emment-Teller (BET) method and nonlocal density functional theory (NLDFT), respectively.

Electrochemical characterization

Linear polarization, and cyclic voltammetry (CV) measurements were carried out on a CHI660E electrochemical analyzer by a three electrodes configuration. The three-electrode system used for linear polarization test involved the saturated calomel electrode (SCE) (as the reference electrode) and Zn foils (as the working electrode and counter electrode). And the threeelectrode system used for CV test included the SCE (as the reference electrode), Zn foil (as the counter electrode).

The dendrite-inhibition and ion-transmission capabilities of Zn electrodes were investigated in symmetric cells with two identical bare Zn foils and different electrolytes. The ionic conductivity (σ, S m^{-1}) for hydrogel electrolytes (size: 10×10×2 mm^3) was measured via the electrochemical impedance spectroscopy (EIS) measurement ranging from 10^{-2} to 10^5 Hz, and calculated by using the equation S1.

$$\sigma = L/AR \quad \text{(S1)}$$

where L (m), R (Ω), and A (m^2) are the thickness, bulk resistance, and test area of hydrogel electrolytes, respectively.

The Zn^{2+} transference number (t_{Zn}^{2+}) of hydrogel electrolytes was measured by EIS and calculated by the equation S2.

$$t_{Zn^{2+}} = (I_S(\Delta V - I_0R_0))/(I_0(\Delta V - I_SR_S)) \quad \text{(S2)}$$

where I_0 (A), I_s (A), ΔV (V), R_0 (Ω), and R_s (Ω) refer to the initial current, steady-state current, applied polarization voltage, initial charge transfer resistance, and steady-state charge transfer resistance, respectively.

The cycling and rate performances of symmetric cells (area of Zn foil: 1.1304 cm^2, thickness: 0.1 mm) were measured on a NEWARE CT-4008Tn battery tester. The cumulative capacity was calculated following the equation (S3):

$$\text{Cumulative capacity} = \frac{\text{Current density} \times \text{Lifespan}}{2} \quad \text{(S3)}$$

The flexible Zn|CTPHE|V_2O_5 ZIB was assembled employing the V_2O_5 cathode, Zn anode, and CTPHE. The V_2O_5, acetylene black and poly(tetrafluoroethylene) with a mass ratio of 7:2:1 were ultrasonically blended in the mixture of deionized NMP, and dried. The charge capacity at a current density of 0.2 A g^{-1} was read to be 0.796 mAh on the NEWARE CT-4008Tn battery tester . The amount of active material V_2O_5 was 1.4 mg, and the area of V_2O_5 cathode was 0.5024 cm^2. The thickness of the Zn anode in the full battery was 10 μm. Its mass was 8.06 mg, and its area was 1.1304 cm^2. The areal capacity of Zn anode was calculated to be 5.85 mAh cm^{-2}, and that of V_2O_5 cathode was calculated to be 1.58 mAh cm^{-2} according to the following equation S4 and S5.

$$\text{Capacity}_{\text{anode}} = \frac{820\ \text{mAh}^{-1} \times \text{m}}{\text{A}} \quad \text{(S4)}$$

where m is the mass of Zn anode, and A is the area of the Zn anode.

$$\text{Capacity}_{\text{cathode}} = \frac{\text{C}_\text{c}}{\text{A}} \quad \text{(S5)}$$

Where C_c is charge capacity at 0.2 A g^{-1}. A is the area of the V_2O_5 cathode. And thus, The N/P ratio of The flexible Zn|CTPHE|V_2O_5 ZIB was maintained at 3.8 according to the following equation S6.

$$\frac{\text{N}}{\text{P}} = \frac{\text{Capacity}_{\text{anode}}}{\text{Capacity}_{\text{cathode}}} \quad \text{(S6)}$$

The depth of discharge (DOD) was calculated considering both the thickness and mass of the zinc foil. The total theoretical capacity per unit area Q_{total} (mAh cm^2) is calculated using the equation (S7):

$$\text{Q}_{\text{total}} = \text{h} \times \rho \times \text{E} \quad \text{(S7)}$$

Where, h is the thickness of the zinc foil, ρ is the density of zinc (7.14 g cm^3), E is the theoretical specific capacity of zinc (820 mAh g).

The $Q_{discharge}$ is calculated using the equation (S8):

$$\text{Q}_{\text{discharge}} = \text{I} \times \text{t} \quad \text{(S8)}$$

Where I (mA cm^2) indicates the applied current density, t (h) is the discharge time.

The DOD is then calculated using the equation (S9):

$$DOD = \frac{Q_{discharge}}{Q_{total}} \times 100\% \quad \text{(S9)}$$

Where, $Q_{discharge}$ is the discharged capacity per unit area of the battery (mAh cm^2).

For Zn-based half cells, I was set to be 1 mA cm^{-2}, and t was set to be 1 h.

The active material V_2O_5 was 1.4 mg, the energy density (E, Wh kg^{-1}) was calculated based on the mass of active cathode material, and energy density were obtained from the Neware battery test system. The power density (P, Wh kg^{-1}) was calculated as follows:

$$P = 3600\ E / t \quad \text{(S10)}$$

where E is energy density, and t is the time, s.

Quantitative lifecycle assessment data

1. Summary of comparative carbon footprint analysis and qualitative-semiquantitative assessment

(1) Raw Material Acquisition:

The conventional electrolytes rely entirely on the fossil-based materials. Our system integrates the bacterial cellulose (BC), which is a renewable bio-based material with carbon-neutral potential, and can relatively reduce the carbon footprint.

(2) Production & Manufacturing:

A key green advantage lies in the aqueous-phase polymerization (at 60°C) for the preparation of PAM/BC/PAF-6, completely avoiding the use of toxic organic solvents (e.g., DMF, NMP) applied in the traditional syntheses. This eliminated the significant energy consumption and emissions associated with the solvent.

(3) Application performance:

The superior electrochemical performance, particularly the exceptional cycling stability (>7000 hours) and high cumulative capacity, indicates its potentially longer battery service life. This enhanced durability can reduce the environmental impact per unit of energy storage over the full lifecycle, representing its crucial indirect eco-benefit.

(4) End-of-life & disposal:

The BC component offers inherent biodegradability potential, providing a more environmentally sound end-of-life option compared to the persistent, non-biodegradable synthetic polymers, such as PVDF.

2. Preliminary assessment of atom economy and environmental impact scores in PAF-6 Synthesis

Theoretical Atom Economy:

The PAF-6 synthesis reaction is a nucleophilic substitution polymerization of cyanuric chloride with piperazine, eliminating only potassium chloride (KCl) as the byproduct, and the theoretical atom economy is >85% following the calculation equation:

$$\text{Atom Economy (AE)} = \frac{\text{Weight of Desired Product}}{\sum\text{Molecular Weights of All Reactants}} \times 100 \quad \text{(S11)}$$

This indicated that most of the reactant atoms are incorporated into the target product, with minimal waste generation (primarily the inorganic salt KCl), aligning with the green chemistry principle of "waste prevention".

Solvent and synthesis conditions:

The reaction was conducted in anhydrous 1,4-dioxane, which can be properly recovered. The reaction was completed in one step, avoiding the cumulative material consumption and energy expenditure associated with the multi-step syntheses. This pathway is more economic compared to the multi-step catalytic polymerization of traditional polymers, such as poly(ethylene oxide) (PEO).

Byproduct handling:

The byproduct KCl is an inorganic salt with low toxicity in aqueous solution, making it easier to treat or potentially utilize as a co-product. Its environmental risk is significantly lower than that of certain organometallic catalysts or organic byproducts.

Calculations

All quantum chemical calculations were performed employing the Gaussian 16, Revision C.01 software package [1]. The geometric structures of the hydrated zinc ion complexes, $[Zn(H_2O)_5\text{-}X]^{2+}$ (where *x* = 1-3), and the isolated water molecules were fully optimized without any symmetry constraints. To ensure that the obtained structures correspond to true minima on the potential energy surface (rather than transition states), harmonic vibrational frequency analyses were conducted at the same level of theory. All optimized structures were confirmed to have no imaginary frequencies. The electronic structure calculations were carried out using the meta-hybrid Minnesota M06-2X density functional theory (DFT) method [2], which is well-regarded for its good performance in describing main-group thermochemistry, non-covalent interactions, and transition metal systems. The Stuttgart-Dresden effective core potential (SDD) basis set [3,4] was employed for the zinc (Zn) atom. The SDD basis set includes a relativistic effective core potential (RECP) to account for scalar relativistic effects, which are important for heavier elements like zinc. The SMD model is considered a universal solvation model due to its parameterization for a wide range of solvents, including water. Furthermore, empirical dispersion corrections were incorporated using the Grimme's D3 dispersion correction with the original damping function (GD3) [5] to better account for long-range van der Waals interactions, which are crucial in weakly bound complexes like ion-water clusters.

The binding energy (Δ E_bind) for the stepwise addition of a water molecule to the zinc aqua complex was calculated using the following equation:

$\Delta E\_bind = E([Zn(H_2O)_5\_M]^{2+}) - E([Zn(H_2O)_5]^{2+}) - E(M)$

Simulation details and methodology

Molecular dynamics (MD) simulation was performed by Gromacs 2025.1 software.[6] The boxes were built by filling molecules randomly using Packmol[7] program. The force field parameters of Zn^{2+} ions and tip4p water model was got from OPLS-AA force field[8]. RESP atom charges were used to describe electrostatic interactions. Atomic charges of Zn^{2+}, SO^{4-} and others were multiplied by scale factor 0.7 to correct the polarization effect of ions. The molecular force field is consisted of nonbonded and bonded interaction. The nonbonded interaction contains van deer Waals (vdW) and electrostatic interaction. For this simulation, an energy minimization was firstly employed to relax the simulation box. Then, an isothermal-isobaric (NPT) ensemble with a 1.0 fs time step is employed to optimized the simulation box, where the temperature is set to 298 K and the pressure is set to 1.0 atm. The temperature and pressure are kept via the Nose-Hoover thermostat and Parrinello-Rahman barostat, respectively. The NPT optimization time was set to 5.0 ns, which is enough long to obtain a stable box size. Following the NPT simulation, a canonical (NVT) ensemble with 100.0 ns was performed to furtherly optimize the simulation box, the time step is set to 2.0 fs. In all the MD simulation, the motion of atoms was described by classical Newton’s equation, which was solved using the velocity-Verlet algorithm[9].

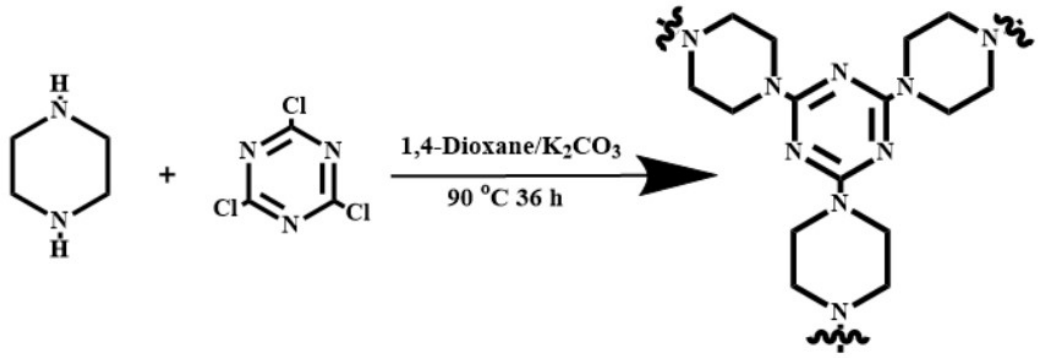

Figure S1. The specific synthesis route of PAF-6.

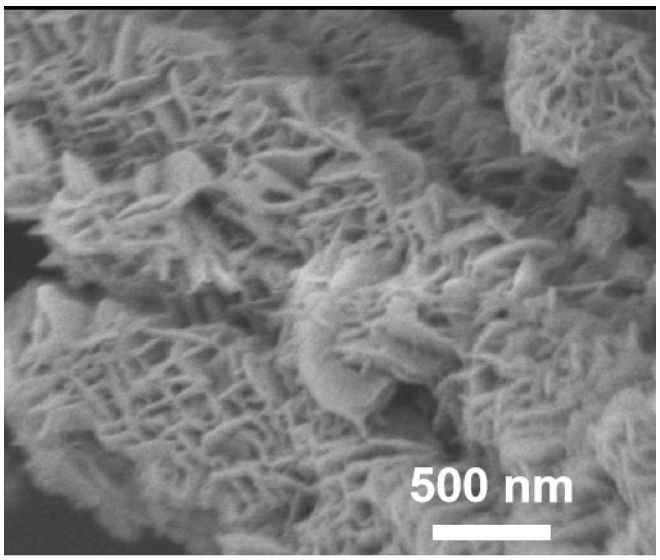

Figure S2. SEM image of PAF-6.

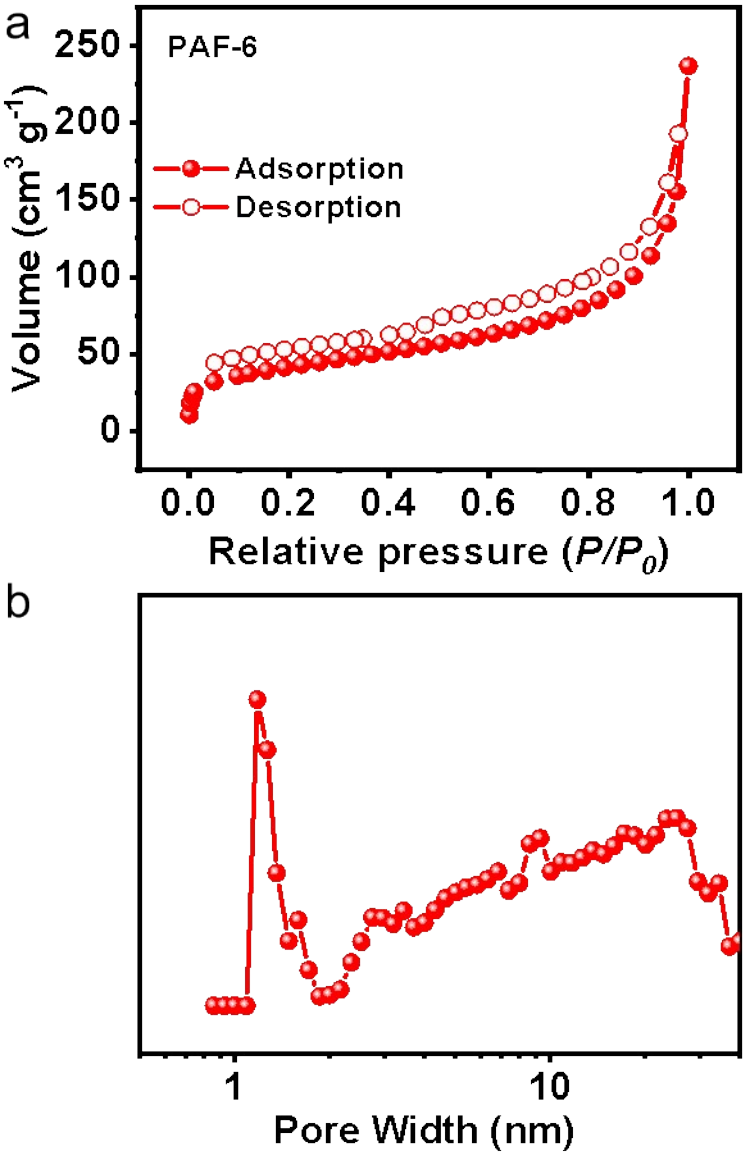

Figure S3. (a) N_2 adsorption/desorption isotherms of PAF-6; (b) Pore distribution of PAF-6.

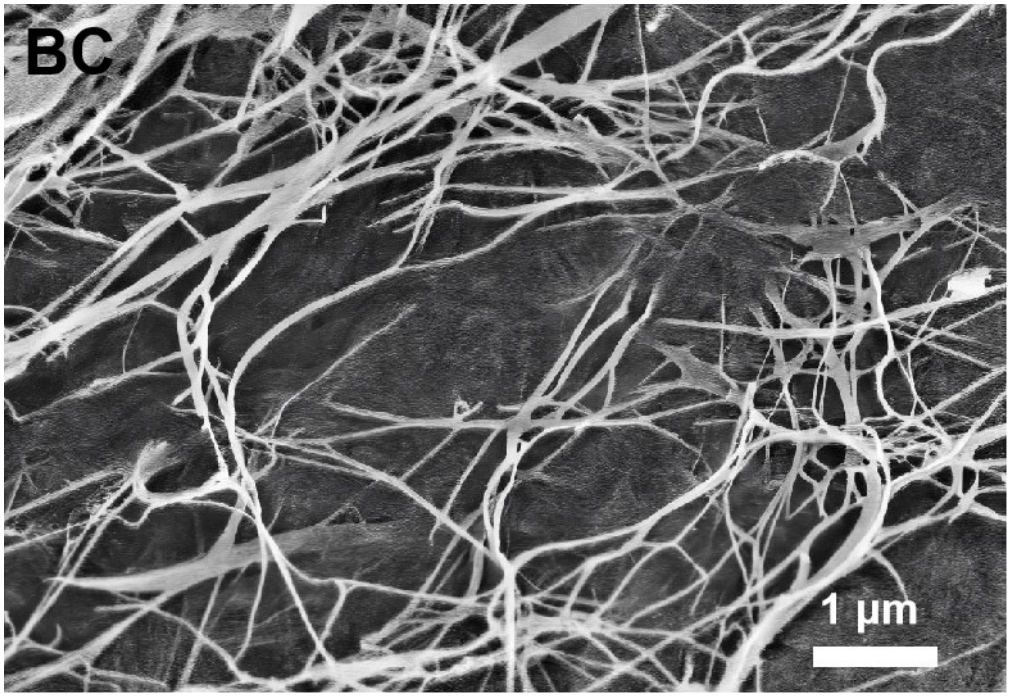

Figure S4. SEM image of BC.

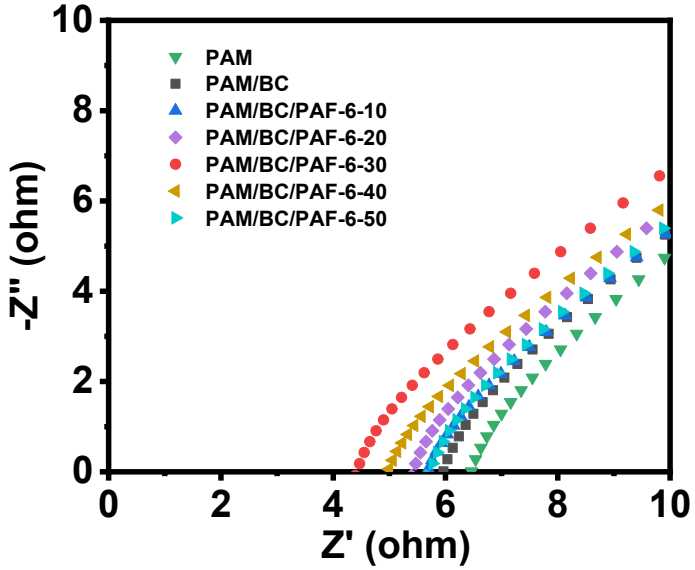

Figure S5. Nyquist plots of PAM, PAM/BC, PAM/BC/PAF-6-10, PAM/BC/PAF-6-20, PAM/BC/PAF-6-30, PAM/BC/PAF-6-40 and PAM/BC/PAF-6-50.

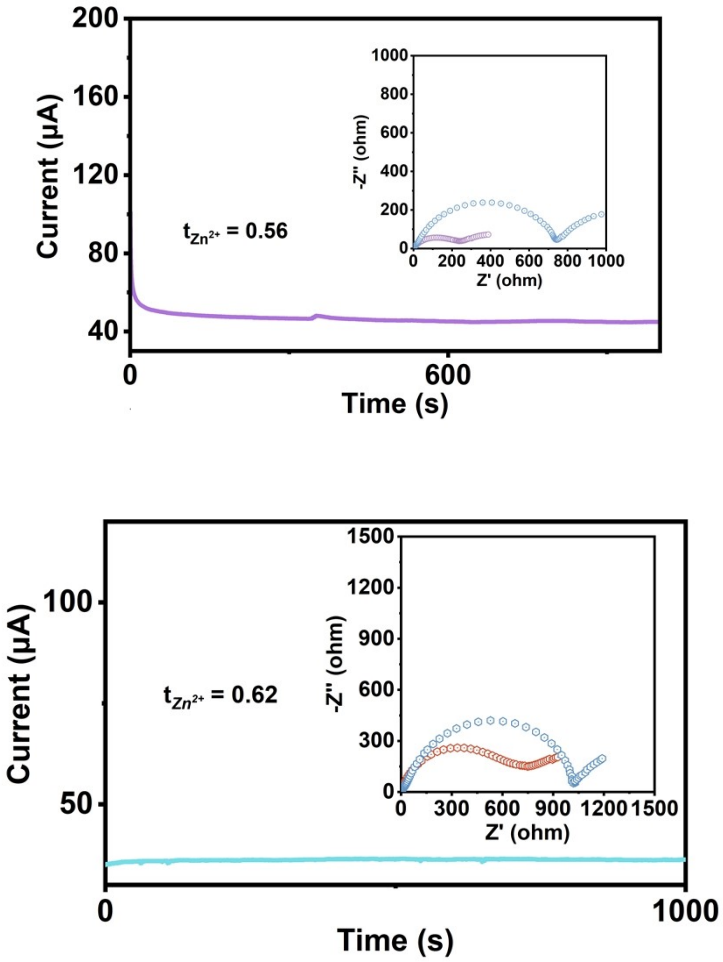

Figure S6. Nyquist plots of symmetric cell with Zn electrodes and PAM, PAM/BC before and after polarization at an applied voltage of 10 mV and the corresponding I-t curve.

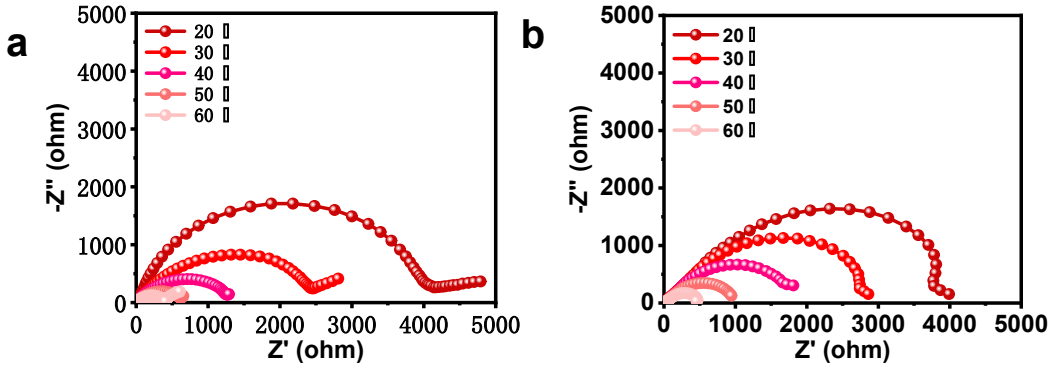

Figure S7. Arrhenius plots for, (a) Zn|PAM/BC|Zn, and (b) Zn|PAM|Zn cells.

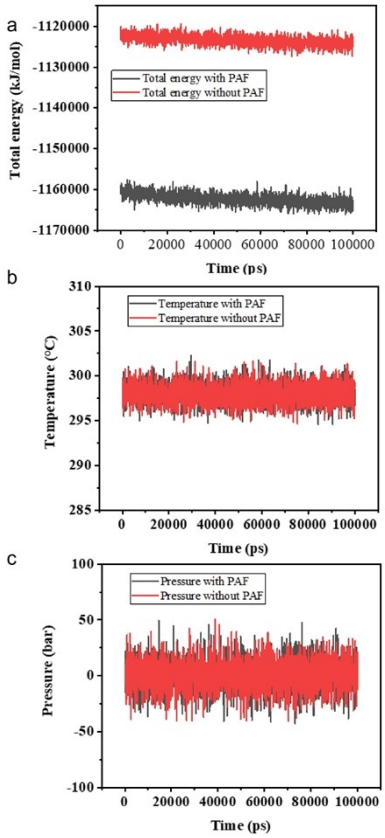

Figure S8. Time evolution of thermodynamic quantities during the NVT equilibration simulation. (a) Total Energy of the system versus time. (b) Instantaneous Temperature of the system versus time. (c) Instantaneous Pressure of the system versus time.

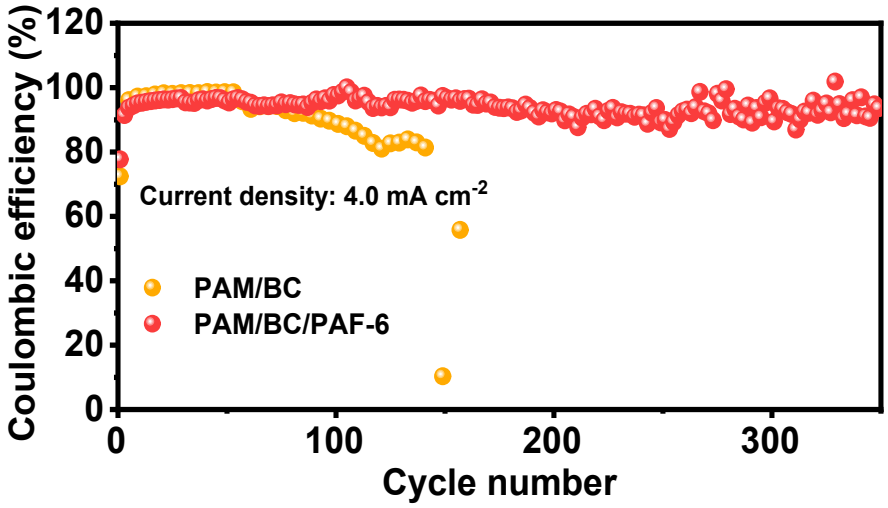

Figure S9. CE of Zn|PAM/BC|Cu and Zn|PAM/BC/PAF-6|Cu cell.

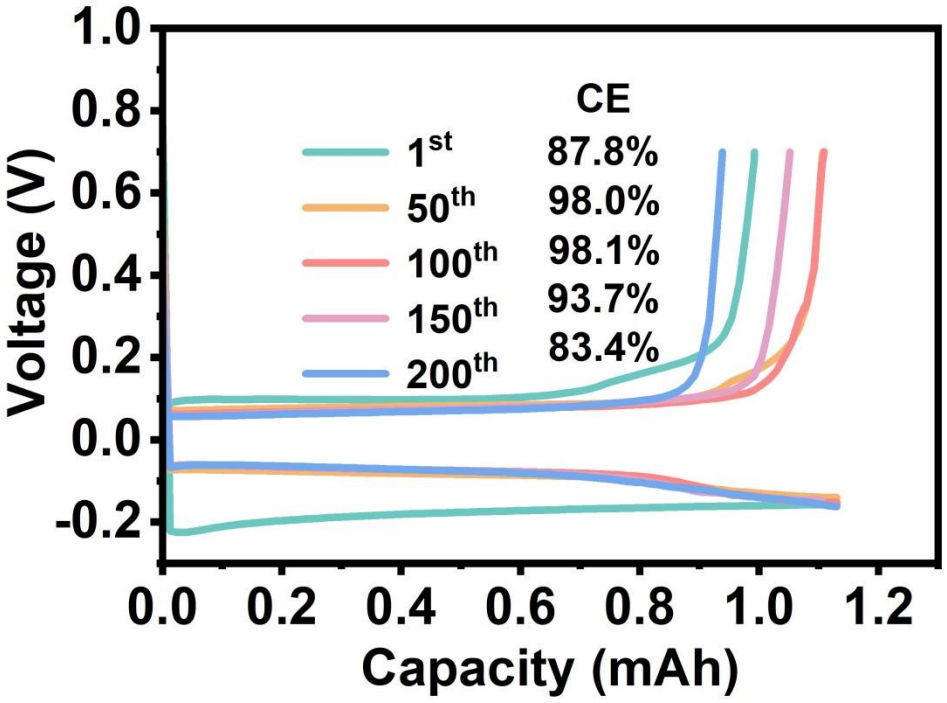

Figure S10. Typical voltage profiles of Zn|CTPHE|Cu cells.

Table S1. Comparison of cumulative capacities for symmetric cells between this work and previous reports with various strategies.

Sample	Current density (mA cm^{-2})	Areal capacity (mAh cm^{-2})	Lifespan (h)	Cumulative capacity (mAh cm^{-2})	Thickness (mm)	References
Zn@SA@Ti	0.5	0.25	2600	650	-	10
LAP@Zn	0.5	0.5	1100	275	-	11
Zn@PAQ	1	1	1750	875	0.01 mm	12
Hedp-Si-Zn	1	1	2000	1000	0.01 mm	13
CF separator	1	1	2000	1000	0.01 mm	14
$ZnSO_4$/TXA	1	1	2000	1000	0.1 mm	15
SAM-Zn	1	0.5	2500	1250	0.1 mm	16
This work	0.5	0.5	7000	1750	0.1 mm	-

Table S2. The capacity retention rate of Zn|PAM/BC/PAF-6|V_2O_5 compared with other reported devices.

Sample	Current density ($A\ g^{-1}$)	Cycle number	Capacity retention rate	References
Zn||V_2O_5	2	1000	75%	17
Zn||PAV	0.2	100	80%	18
PAN||Zn	0.5	1000	82.7%	19
Zn||V_2O	0.1	1000	81%	20
This work	1	600	85.1%	

[1] Gaussian 16, Revision C.01, Frisch, M. J.; et al. Gaussian, Inc., Wallingford CT, (2016).

[2] Zhao, Y.; Truhlar, D. G. The M06 Suite of Density Functionals for Main Group Thermochemistry, Thermochemical Kinetics, Noncovalent Interactions, Excited States, and Transition Elements: Two New Functionals and Systematic Testing of Four M06-Class Functionals and 12 Other Functionals. Theor. Chem. Acc. 120 (2008) 215–241.

[3] Andrae, D.; Häußermann, U.; Dolg, M.; Stoll, H.; Preuß, H. Energy-Adjustedab Initio Pseudopotentials for the Second and Third Row Transition Elements. Theor. Chim. Acta 77 (1990) 123–141.

[4] Bergner, A.; Dolg, M.; Küchle, W.; Stoll, H.; Preuß, H. Ab Initio Energy-Adjusted Pseudopotentials for Elements of Groups 13–17. Mol. Phys. 80 (1993) 1431–1441.

[5] Grimme, S.; Antony, J.; Ehrlich, S.; Krieg, H. A Consistent and Accurate Ab Initio Parametrization of Density Functional Dispersion Correction (DFT-D) for the 94 Elements H-Pu. J. Chem. Phys. 132 (2010) 154104.

[6] B. Hess and C. Kutzner and D. van der Spoel and E. Lindahl, GROMACS 4: Algorithms for highly efficient, load-balanced, and scalable molecular simulation, J. Chem. Theory Comput. 4 (2008) pp. 435-447.

[7] Martinez, L.; Andrade, R.; Birgin, E. G.; Martinez, J. M., PACKMOL: a package for building initial configurations for molecular dynamics simulations. J. Comput. Chem. 30 (2009) 2157-64.

[8] Nosé, S., Klein, M. L., Constant. Molecular Physics 5 (1983) 1055-1076.

[9] Darden, T., York, D., Pedersen, L., J. Chem. Phys. 12 (1993) 10089-10092.

[10] H. Zhang, Y. Wu, J. Yu, T. Jiang, M. Wu, *Adv. Funct. Mater.* 2023, **34**, 2301912.

[11] J. Feng, X. Li, X. Cui, H. Zhao, K. Xi, S. Ding. *Adv. Energy Mater.* 2023, **21**, 2204092.

[12] D. Xie, Z. Wang, Z. Gu, W. Diao, F. Tao, C. Liu, H. Sun, X. Wu, J. Wang, J. Zhang, *Adv. Funct. Mater.* 2022, **32**, 2204066.

[13] H. Yu, Y. Chen, H. Wang, X. Ni, W. Wei, X. Ji, L. Chen, *Nano Energy* 2022, **99**, 107426.

[14] W. Zhou, M. Chen, Q. Tian, J. Chen, X. Xu, C. Wong, *Energy Storage Mater.* 2022, **44**, 57-65.

[15] J. Yin, H. Liu, P. Li, X. Feng, M. Wang, C. Huang, M. Li, Y. Su, B. Xiao, Y. Cheng, X. Xu. *Energy Storage Mater.* 2023, **59**, 102800.

[16] D. Li, Y. Tang, S. Liang, B. Lu, G. Chen, J. Zhou. *Energy Environ. Sci.* 2023, **8**, 3381-3390.

[17] H. Wang, A. Zhou, Z. Hu, X. Hu, F. Zhang, Z. Song, .Y. Huang, Y. Cui, . Y. Cui, L. Li, F.Wu, R.Chen, *Angew. Chem. Int. Ed.* 2024, **136***,* e202318928.

[18] R. Li, F. Xing, T. Li, H. Zhang, J. Yan, Q. Zheng, X. Li, *Energy Storage Mater.* 2021, **38**, 590–598.

[19] Y. Liu, C. Lu, Y. Yang, W. Chen, F. Ye, H. Dong, Y. Wu, R. Ma, L. Hu, *Adv. Mater.* 2024, **36**, 2312982.

[20] S. Chen, D. Ji, Q. Chen, J. Ma, S. Hou, J. Zhang, *Nat. Comm.* 2023, **14**,3526.